Integrative Biology

RSC Publishing

PAPER

View Article Online
View Journal

Guidance of collective cell migration by substrate geometry†

Cite this: DOI: 10.1039/c3ib40054a

Kevin Doxzen,‡[a] Sri Ram Krishna Vedula,‡[a] Man Chun Leong,[b] Hiroaki Hirata,[a] Nir S. Gov,[c] Alexandre J. Kabla,[d] Benoit Ladoux*[ae] and Chwee Teck Lim*[af]

Received 11th March 2013,
Accepted 22nd May 2013

DOI: 10.1039/c3ib40054a

www.rsc.org/ibiology

Collective behavior refers to the emergence of complex migration patterns over scales larger than those of the individual elements constituting a system. It plays a pivotal role in biological systems in regulating various processes such as gastrulation, morphogenesis and tissue organization. Here, by combining experimental approaches and numerical modeling, we explore the role of cell density ('crowding'), strength of intercellular adhesion ('cohesion') and boundary conditions imposed by extracellular matrix (ECM) proteins ('constraints') in regulating the emergence of collective behavior within epithelial cell sheets. Our results show that the geometrical confinement of cells into well-defined circles induces a persistent, coordinated and synchronized rotation of cells that depends on cell density. The speed of such rotating large-scale movements slows down as the density increases. Furthermore, such collective rotation behavior depends on the size of the micropatterned circles: we observe a rotating motion of the overall cell population in the same direction for sizes of up to 200 μm. The rotating cells move as a solid body, with a uniform angular velocity. Interestingly, this upper limit leads to length scales that are similar to the natural correlation length observed for unconfined epithelial cell sheets. This behavior is strongly altered in cells that present a downregulation of adherens junctions and in cancerous cell types. We anticipate that our system provides a simple and easy approach to investigate collective cell behavior in a well-controlled and systematic manner.

Insight, innovation, integration

Collective cell behavior plays a crucial role in various biological processes such as gastrulation, wound healing and cancer metastasis. While it is accepted that physical cues within the extracellular microenvironment are known to influence cell migration, a systematic and comprehensive insight into their role in governing collective cell behavior is lacking. In this study, we have integrated microcontact printing techniques with particle image velocimetry, live-cell imaging and numerical simulations to systematically probe how geometrical constraints imposed by the substrate altered intercellular adhesion and cell density guide and regulate collective cell behavior.

Introduction

Collective behavior refers to a phenomenon in which, under certain conditions, complex migration patterns evolve over scales that are much larger than those of the individual constituents making up a given system.[1–5] It is now well recognized as a universal phenomenon that is observed in a variety of systems (physical, chemical and biological) constituted of microscopic (*e.g.* molecules, cells) as well as macroscopic (*e.g.* fish, birds) elements.[2,6,7] Collective behavior of cells is particularly interesting because of its role in influencing physiological processes such as development, morphogenesis, and organization of complex tissues[8–10] as well as pathological processes such as cancer cell invasion.[11] Much attention has been paid to understand the mechanics of individual cells[12] but little is known about the mechanisms that drive collective cell behaviors. Furthermore, results from single cell studies could not be directly used to capture the dynamics of multicellular systems since collective interactions create more complex dynamics

[a] *Mechanobiology Institute, National University of Singapore, Singapore 117411*
[b] *NUS Graduate School for Integrative Sciences and Engineering, National University of Singapore, Singapore 117576*
[c] *Department of Chemical Physics, Weizmann Institute of Science, Rehovot 76100, Israel*
[d] *Engineering Department, University of Cambridge, Cambridge, UK*
[e] *Institut Jacques Monod (IJM), CNRS UMR 7592 & Université Paris Diderot, Paris, France. E-mail: benoit.ladoux@univ-paris-diderot.fr*
[f] *Department of Bioengineering & Department of Mechanical Engineering, National University of Singapore, Singapore. E-mail: ctlim@nus.edu.sg*

† Electronic supplementary information (ESI) available. See DOI: 10.1039/c3ib40054a

‡ Equal contribution.

than the sum of the parts.[13,14] Thus, the adhesive state between cells is critical for collective cell migration and must be very carefully regulated. High cohesiveness is frequently associated with a decrease in speed, as it has been shown that knocking down adhesive proteins leads to an acceleration of migration.[15] Moreover, it is recurrently observed that epithelial cells can slide past each other and change neighbors while moving collectively and cohesively.[16] Several mechanisms have been suggested including cell–cell interactions and formation of leader cells that are supposed to guide the rest of the cohort.[17] Moreover, other studies have reported the presence of cryptic lamellipodia in cells located many rows away from the leading edge, challenging the notion of only leader extending protrusions[18] and suggesting additional modes of migration through self-movements.

In view of the crucial role that collective cell behavior plays in regulating various biological phenomena, numerous efforts have been made to identify the various physico-chemical factors that influence collective cell behaviors[19–23] as previously done for single cell studies.[24–26] For instance, it has been shown that cell density and substrate deformation patterns regulate collective migration patterns in large expanding cell sheets.[27] Other studies have characterized the influence of geometrical constraints (curvature and size of the confinement) on the emergence of leader cells[28] and their role in collective behavior.[29,30] Based on such studies, it clearly appears that biological processes driven by the interactions of multiple cells involve the coordination of cell displacements across large length scales and time scales.[31–33]

Recently, a phenomenon termed 'coherent angular motion' (CAM) has been described in breast epithelial cells growing within 3D collagen matrices.[34] CAM refers to the manner in which epithelial cells in 3D collagen gels undergo synchronized collective rotation and has been proposed to play an important role in determining the formation of acini and ducts in glandular tissue, tissue polarity and embryogenesis.[34] Interestingly, CAM was not observed in cancerous cells and cells incubated with function blocking antibodies against E-cadherin suggesting that intercellular adhesion is important in regulating such rotation. Furthermore, studies also suggest that collective synchronized migration of cells is also regulated by the intrinsic chirality of cell types and might play an important role in determining left–right symmetry during organogenesis.[35]

Despite a wealth of data provided by these studies, a systematic and comprehensive evaluation of the major factors influencing collective cell behavior is lacking. Here, we have combined experimental techniques that include microfabrication techniques and particle image velocimetry (PIV) together with numerical modeling to characterize the influence of cell density, geometrical constraints and intercellular adhesion on collective behavior of MDCK epithelial cell sheets. The configuration studied here is a version of the two-cell experiments previously described by Ingber *et al.*[36] To further put our results in perspective, we show that MDCK cells that have undergone epithelial to mesenchymal transition (EMT), as well as different types of breast cancer cells, show either inefficient or complete inability to participate in large scale synchronized collective migratory behavior. We propose that the loss of collective behavior in cancer cells could partially underlie their inability to form higher order tissue structures such as glands and ducts.

Results

MDCK cells undergo synchronized, collective rotation after reaching a critical density

Previous studies on collective behaviors of various systems including passive physical interactions or active matter have established that the density of constituent elements is a key regulator of the emergence of large scale correlated migration patterns.[1,3,4] We first investigated how cell density regulated the emergence of collective behavior in MDCK cells. To do so, we seeded cells at very low density ($\sim$800 cells per mm^2) on microcontact printed (μCP) circular fibronectin patterns that were $\sim$200 μm in diameter. Phase contrast images, as well as fluorescent images, of the nuclei were obtained for $\sim$48 hours until cells reached very high densities ($\sim$10 000 cells per mm^2). The videos were only analyzed up to a density of 6000 cells per mm^2 because at higher densities MDCK cells began to grow over each other making the PIV analysis of videos inaccurate. μCP fibronectin patterns restricted cells from migrating out of the field of view, making it easier to image and analyze the migration characteristics. Under these conditions, with increasing cell density, distinct phases of cell migration behavior were observed. At very low densities (below confluence), cells were distributed sparsely as single cells or small clusters and have a tendency to migrate randomly. While small clusters of cells did show transient ordered migratory behavior, it was lost quickly as cells spread out to fill up the free space (Fig. 1a, Video S1, ESI†). Immediately after confluence, cells migrated in a synchronized and collectively rotating pattern, as a rotating solid-body (Fig. 1b, Video S2, ESI†). At higher cell densities, collective rotation behavior persisted but the average velocity of the cells decreased (Fig. 1c, Video S3, ESI†). The synchronized and persistent rotation was highly reminiscent of CAM described in breast epithelial cells growing in 3D collagen gels.[34] Since cells are able to decorate the initial ligand with additional ECM proteins, we analyzed if the coordinated movement of cells could be due to changes in the composition of ECM in the patterns. To do so, cells were first allowed to reach complete confluence on the patterns ($\sim$48 hours after seeding). Subsequently, cells were removed using an enzyme free cell dissociation buffer (GIBCO) and the patterns were repopulated with freshly sub-cultured cells. Under these conditions, coordinated rotational motion of the cells was observed only when they reached a confluent state (Movie S4, ESI†). This result demonstrates that the dynamics of coordinated movements could not be attributed to changes in ECM coating over time and is rather related to cell–cell interactions.

We used PIV for quantitative characterization of these phases.[32] The spatial average of all the velocity vectors within the fibronectin pattern ($V_{avg} = \langle|V_i|\rangle$) was plotted as a function of cell density (Fig. 1d). We divided the evolution of the migratory characteristics into three phases based on this plot (Fig. 1d). The first or sub-confluent phase, when cell density is $<$2000 cells per mm^2, is characterized by a low V_{avg} and uncorrelated velocity vectors.

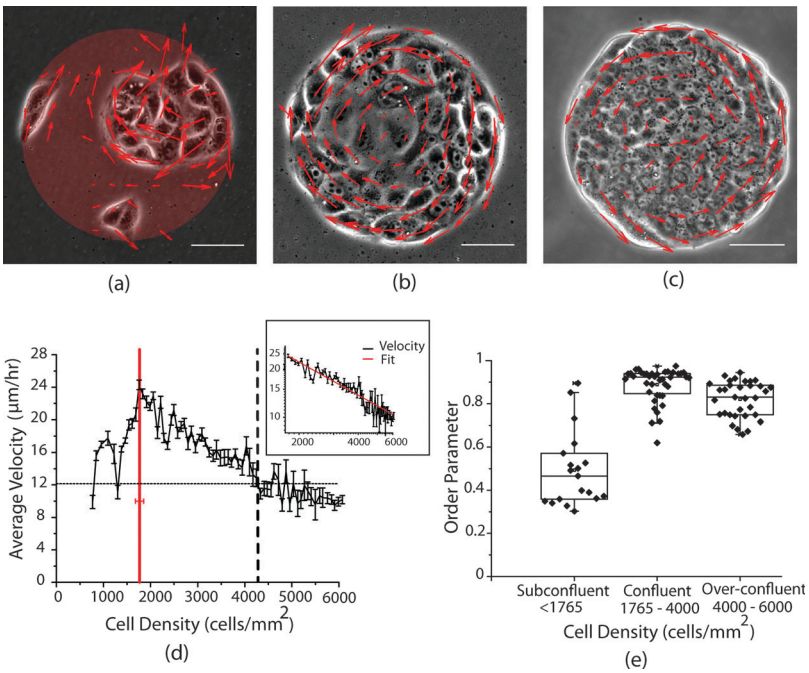

Fig. 1 MDCK cells seeded on circular fibronectin patterns 200 μm in diameter and analysed using particle image velocimetry (PIV). Red arrows represent the magnitude and direction of local velocity fields. (a) Cells in a sub-confluent state, (b) cells reaching confluence at ~2000 cells per mm^2, (c) cells at a very high density of ~4000 cells per mm^2, and (d) change in average velocity V_{avg} with increasing cell density. The red vertical line represents the average cell density at which confluence is reached (see methods) and the black dotted vertical line represents the density at which V_{avg} is approximately half of its maximum. Inset: decrease in average velocity with increasing density on a log–log plot. The slope of the linear fit is 0.7. (e) Evolution of the order parameter with increasing cell density. Low order parameter in the sub-confluent state reflects random migration of cells. Order sets at a critical density of ~2000 cells per mm^2. In the over-confluent state, the order parameter shows a broader distribution. Scale bar = 50 μm.

The second phase, characterized by the onset of collective synchronized rotation of cells and high V_{avg} (~25 μm h^{-1}), is triggered when a critical density of ~2000 cells per mm^2 is reached. In the third or over-confluent phase, cell densities reach values >4000 cells per mm^2 and V_{avg} falls below approximately half of its maximum value. These three phases are not unique to cells grown on circular micropatterns and have been described previously in the context of scratch wound assays[37] and large expanding cell sheets.[7] For example, single as well as small islands of MDCK cells migrate very little and tend to expand primarily as a result of proliferation. Collective migration of the monolayer ensues only after a 'threshold-density' is reached.[37] Interestingly, the 'threshold-density' reported for monolayer migration is similar to the density at which cells undergo collective rotation on circular patterns (~2000 cells per mm^2). Furthermore, a decrease in the V_{avg} to approximately half of its maximum at cell densities >4000 cells per mm^2 has been observed in expanding MDCK cell sheets and coincides with their transition into a 'glassy' phase and the inhibition of lamellipodia protrusion.[7] The decrease in the average velocity with increasing density can be modeled as a balance between cell traction forces exerted through lamellipodia (F_{tract}) and frictional forces between the cell and the substrate (F_{fric}). Such a balance predicts that the average velocity will decrease as the square root of cell density (ESI†). Indeed, a log–log plot of the average velocity with density (after reaching confluence) showed a linear relation with a slope of ~0.7 (Fig. 1d, inset) that is comparable to the predicted value. The faster decay observed experimentally could arise from other changes such as increase in friction over time or altered lamellipodial formation.

In order to further quantify the collective cell behavior, we computed the average order parameter from the PIV analysis for the three phases to quantify the organization of the cell sheet (see Experimental section).[30] Briefly, an order parameter equal to one signifies that the velocity vector is perpendicular to the radius vector. It was observed that the average order parameter was (0.49 ± 0.17) in the sub-confluent phase, increased to (0.88 ± 0.08) in the collective rotation phase and decreased to (0.82 ± 0.08) while showing a relatively broad distribution during the over-confluent phase (Fig. 1e). This correlated well with the random migration of cells in the sub-confluent phase, highly ordered collective behavior in the confluent phase and partially ordered migration at high densities.

Effect of ECM constraints on the synchronized collective rotation behavior of cells

We hypothesized that the emergence of a synchronized collective rotation behavior is also regulated by the size of confinements within which the cells are allowed to migrate. Accordingly we analyzed the migratory behavior of cells on circular fibronectin patterns with diameters of 100, 200, 500 and 1000 μm. Interestingly, the synchronized collective rotation of the whole cell sheet at a critical density of ~2000 cells per mm^2 was observed only in the 100 and 200 μm diameter patterns

(Fig. 2a and b, Videos S2 and S5, ESI†). In the 500 and 1000 μm diameter patterns, transient vortices ~300 μm in diameter were observed that closely resembled the collective rotation observed in the 100 and 200 μm diameter patterns (Fig. 2c, Video S6, ESI†). To further investigate this phenomenon, we computed the average spatial correlation of velocity vectors obtained using PIV for patterns of different diameters when the cell density was ~2000 cells per mm^2. For the 100 and 200 μm diameter patterns, spatial correlation reached zero at ~50 and 100 μm, respectively, and continued to become negative at larger length scales signifying the synchronized collective rotation behavior of the whole cell sheet (Fig. 3a). The curve obtained is in fact very close to the measured correlation function of the velocity field of a simulated solidly rotating disk of equivalent size (dashed fit, Fig. 3a) exhibiting a synchronous movement of the monolayer. On the other hand, the correlation value reached zero at ~170 μm for both 500 and 1000 μm diameter patterns suggesting that a saturation regime has been reached (Fig. 3a and b). Furthermore, the spatial correlation did not show significant negative values corroborating the fact that there was no synchronized collective rotation of the whole cell sheet. Interestingly, this correlation length correlates well with that observed for unconfined MDCK monolayers and probably represents the natural correlation length arising from internal tissue dynamics.[28] Together, these results suggest that synchronized collective rotation of the whole cell sheet (akin to CAM)[34] occurs only over length scales that are smaller or approximately the same size as the natural correlation length of the unconfined epithelial monolayer.

Based on these observations, we hypothesized that the rotation of the cellular clusters could be described as a purely

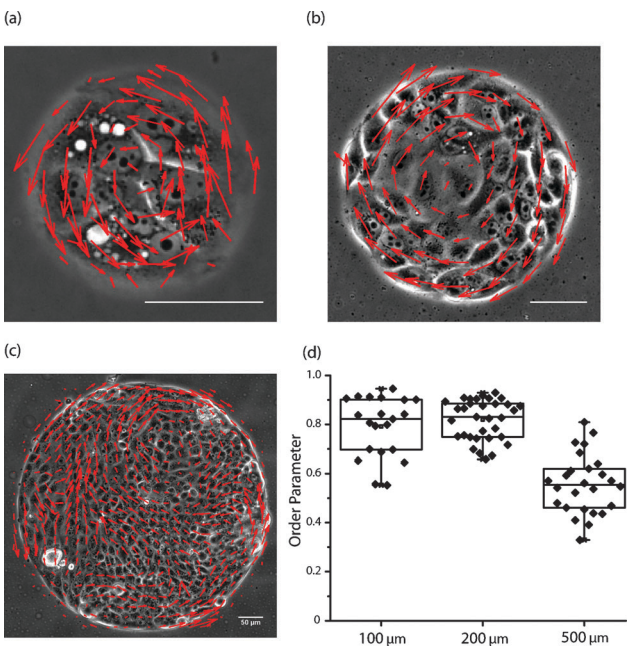

Fig. 2 PIV analysis of the collective behavior of MDCK cells at confluence on circular fibronectin patterns with a diameter of (a) 100, (b) 200 and (c) 500 μm. (d) Average order parameter in patterns with a diameter of 100, 200 and 500 μm at confluence.

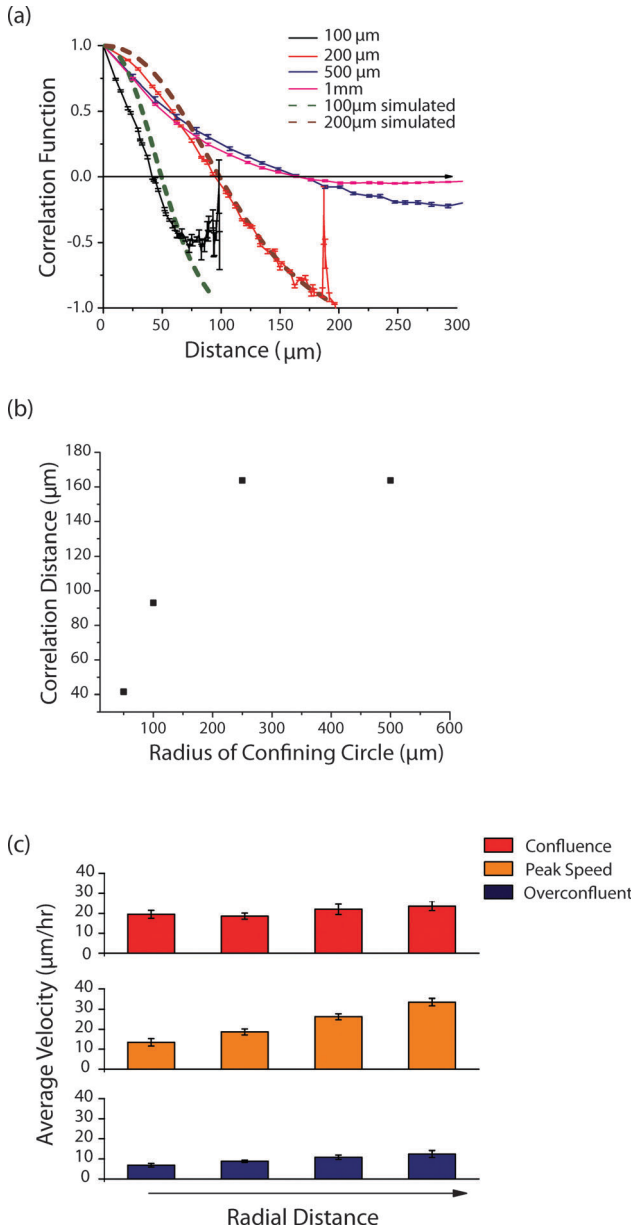

Fig. 3 (a) Spatial correlation of velocity vectors as a function of distance. The dashed lines represent the velocity correlations obtained for simulated solidly rotating discs of equivalent sizes, (b) correlation length as a function of the radius of the circular fibronectin pattern, (c) average velocities at different distances (spaced 25 μm apart) from the centre for confluent, peak speed and over confluent phases in a 200 μm diameter circle. Scale bar = 50 μm.

solid-like cluster. Consider a circular cluster of cells in two dimensions, of radius R, treated as a solid object with all the cells therefore moving coherently together. However, the individual traction forces produced by the cells may not be correlated and can be randomly oriented, or they may be correlated with the cell's neighbors. Cell–cell correlations are evident in collective cellular motion.[23,38] We characterize the active forces induced by the individual cells as having a typical force f_0, a mean burst length T_{noise} (persistence time of the cellular traction force) and mean waiting time between bursts T.[39] If all the cells are

correlated inside the cluster, then all the traction forces point in the azimuthal direction (the radial component is removed by the fact that the cells are confined to an isolated island). The overall torque applied by the cells is then given by

$$T_{\text{active}} = f_0 \int_0^R \frac{2\pi r}{A_{\text{cell}}} r \mathrm{d}r = \frac{2\pi}{3A_{\text{cell}}} f_0 R^3$$

where A_{cell} is the area of a single cell. This active torque due to the cellular tractions has to be balanced by the total frictional torque, which is given by

$$T_{\text{friction}} = \lambda_0 \int_0^R 2\pi r(r\omega) r \mathrm{d}r = \frac{\pi}{2} \lambda_0 R^4 \omega$$

where λ_0 is the friction per unit area. From these two equations we compute the angular velocity, ω, of the solid-like cellular layer:

$$\omega = \frac{4f_0}{3\lambda_0 A_{\text{cell}}} \frac{1}{R}$$

The angular rotation of a purely solid-like cluster decreases as $1/R$, which makes the velocity at the edge of the cluster a constant independent of the cluster size: $v_{\text{edge}} = R\omega = \text{const}$.

We then compared our model with the experiments for 100 and 200 μm. We indeed observed comparable velocities at the rim of the circles for both diameters (26.35 ± 1.4 and 33.49 ± 1.8 μm h^{-1} respectively). Moreover it appeared that the velocity along the radial direction varied linearly with the radial position, which is in agreement with our solid-like model (Fig. 3c).

Numerical results from a confined confluent monolayer

In an effort to directly test the role of confinement in the dynamics of a generic collective migrating system, we also implemented a computational model based on simple cellular behavior (cell–cell cohesion, cell–substrate motile forces and persistence time cell polarization). Simulations show that groups of cells develop coordination even before confluence is reached, although the migratory patterns are continuously evolving over time due to the lack of interaction with the pattern boundaries (Video S7, ESI†). Cells underwent a persistent solid rotation when they were confined to a disc whose size was smaller than or equal to the correlation length for the system (Fig. 4a, Video S8, ESI†). At larger length scales (larger disc sizes), cells formed local swirls but global coordination was not achieved (Fig. 4b and c, Videos S9 and S10, ESI†). Such a transition in collective cell behavior beyond length scales larger than the correlation length is reminiscent of the size effects observed *in vitro* and *in silico* in migrating cell sheets subjected to varying degrees of confinement.[30,40] The correlation function (Fig. 4d) and correlation length (Fig. 4e) in the steady state were calculated as a function of the disc radius. We find trends consistent with experimental observations and a good quantitative agreement for a system calibrated to have an unconfined correlation length comparable to the experimental measurements. These observations show that the rotational order emerging in these cell populations is likely to be a generic feature of confined coordinated cells. Factors influencing the correlation length or the ability to correlate remain to be explored.

Role of intercellular adhesion in regulating collective rotation behavior

Intercellular adhesion plays a key role in regulating the migration characteristics of epithelial cells. In particular, our previous study[30] showed that the migration of MDCK cells that cannot form stable intercellular contacts was highly uncoordinated and hence, led to significantly lower migration velocity. This is evident from the fact that cells that undergo epithelial to mesenchymal transition (EMT), a hallmark of many carcinomas, exhibit altered migratory behavior and decreased expression of intercellular adhesion molecules.[41]

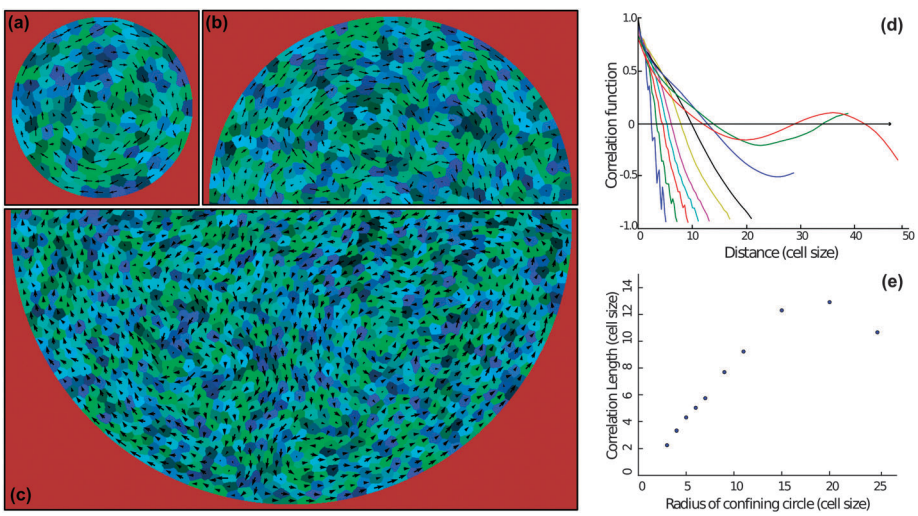

Fig. 4 Numerical simulations of the migratory behavior of epithelial cells confined to discs of different sizes. (a) Global rotation occurs when discs are smaller than or equal to the size of the natural correlation length of cells. (b and c) For larger discs, local streams and curls are observed but global coordination does not set in. (d) Spatial velocity correlation as a function of distance obtained in the numerical simulations. (e) Correlation length increases linearly for small confinements but saturates at length scales larger than the natural correlation length of the unconfined monolayer.

We hypothesized that cells that have undergone EMT would be unable to exhibit a synchronized collective rotation behavior due to their inability to form mature intercellular contacts. To test this hypothesis, we used MDCK cells stably overexpressing the transcription factor Snail-1. Overexpression of Snail-1 in MDCK cells has previously been shown to downregulate E-cadherin expression, impart a mesenchymal phenotype to the cells (EMT), decrease the cell proliferation rate and increase spreading on fibronectin.[42–45] Western blot of Snail-1-MDCK cells indeed showed that the expression of E-cadherin was completely suppressed while the expression of α-catenin was strongly downregulated (Fig. S1, ESI†). When seeded on 200 μm diameter circular fibronectin patterns, Snail-1-MDCK cells exhibited increased spreading and thus reached confluence at a much lower density (~600 cells per mm^2) than wt-MDCK (~2000 cells per mm^2) (Fig. 5a). Interestingly, while Snail-1-MDCK cells did show a collective rotation behavior after reaching confluence, the rotation itself was transient (~8 h) compared to the persistent rotation observed in wt-MDCK cells (>25 h). After a short period of rotation, cells changed direction and started to rotate in the opposite direction (Video S11, ESI†). PIV analysis of Snail-1-MDCK cells at densities >1800 cells per mm^2 was not possible as the cells had a tendency to migrate over one another. Within this range, the change in V_{avg} as a function of cell density showed a trend similar to that observed in wt-MDCK cells (Fig. 5b). However, in contrast to wt-MDCK cells, the order parameter for the Snail-1-MDCK cells showed an oscillatory behavior with time reflecting the changes in the direction of rotation of the cell sheet (Fig. 5c and d, Video S11, ESI†). This was especially more evident in cells closer to the edge of the pattern while cells in the centre moved much more randomly (Fig. 5c). Furthermore, manual tracking of the nuclei showed that Snail-1-MDCK cells, unlike wt-MDCK, had a tendency to move from the edge of the pattern into the centre

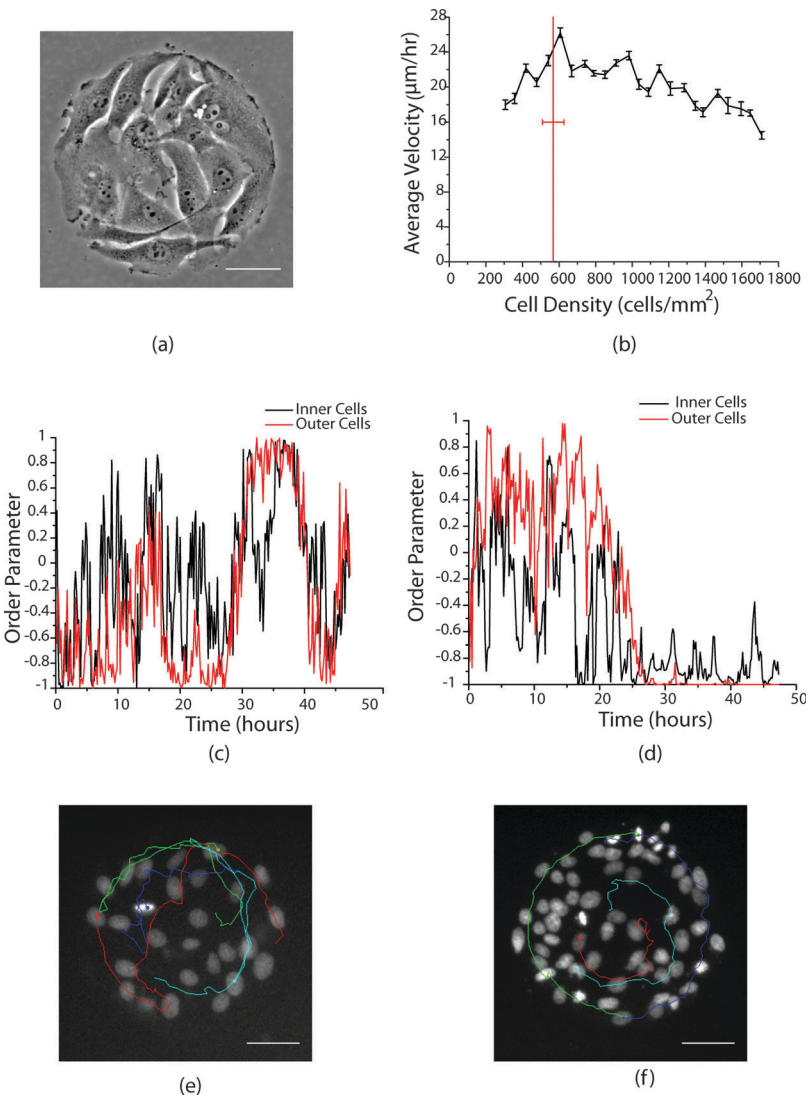

Fig. 5 (a) Snail-1-MDCK cells on 200 μm diameter circular fibronectin patterns reach confluence at much lower density, and (b) V_{avg} as a function of cell density. Temporal evolution of the order parameter in (c) Snail-1-MDCK and (d) wt-MDCK cells. Tracking nuclei of (e) Snail-1-MDCK and (f) wt-MDCK cells showing that Snail-1-MDCK cells have a tendency to migrate from the edge of the pattern into the centre. Scale bar = 50 μm.

and *vice versa* (Fig. 5e and f, Videos S12 and S13, ESI†). It is not straight-forward to realistically model the behavior of Snail-1-MDCK cells within our framework; the decreased intercellular adhesion and increased spreading of Snail-1-MDCK cells on the substrate result in lower density at confluence and very dynamic fluctuations of the cell area on the substrate. Experimental observations (Movie S10, ESI†) suggest however that the system could be modeled as a population of non-cohesive sub-confluent entities. We therefore studied the dynamics of non-cohesive sub-confluent cell population (see Methods). Results show that for moderate cell densities (70% coverage), coordination can emerge despite the lack of adhesion, but it is fragile and transient leading to changes in the direction of rotation of the overall population (Video S14, ESI†), as observed experimentally. Although the experimental observations at confluence currently cannot be explained by the model, the complex dynamics observed in Snail-1-MDCK cells can partly be accounted for by a change in cell–cell adhesion and decrease in cell density.

To compare and correlate our experiments on wt-MDCK and Snail-1-MDCK cells with different patho-physiological conditions, we studied the migratory behavior of MCF-10A (derived from a benign breast tumor), MCF-7 and MDA-MB-231 cells (derived from a malignant tumor) on 200 μm diameter fibronectin patterns. Interestingly, MCF-10A cells separated frequently from their neighbors, suggesting weak intercellular adhesion. They also spread more, and showed a phenotype very similar to that of Snail-1-MDCK cells (Video S15, ESI†) but migrated slower than Snail-1-MDCK cells. While the outer cells in contact with the edge of the micropattern exhibited some degree of collective rotation at confluence, cells in the centre migrated randomly (Fig. 6a). Such a behavior can be explained by assuming that the outer cells are being guided by the edge of the micropattern, a phenomenon described as 'contact guidance'.[46] However, it is likely that synchronized collective rotation of all cells within the pattern requires mature intercellular adhesion that MCF-10A cells lack. On the other hand, both MCF-7 and MDA-MB-231 cells showed a random and chaotic movement with no tendency to undergo collective behavior such as large scale rotating movements at any given cell density (Fig. 6b and c, Videos S16 and S17, ESI†). These results suggest that the loss of collective behavior could be a gradually occurring event during the evolution of cells from normal to a malignant phenotype.

Discussion and conclusion

We have performed a systematic and comprehensive analysis of the influence of cell density, geometrical constraints and EMT on collective behavior in epithelial cells by combining μCP and PIV. Miniature epithelial monolayers on micropatterns, as opposed to large monolayers, provide a reproducible platform to characterize the role of cell density, geometric constraints and boundary effects in collective cell behavior. Our results suggest that reaching a critical density ($\sim$2000 cells per mm^2) triggers collective behavior in MDCK cells. The influence of the density on the appearance of collective behavior has been clearly established in many other biological systems such as actin filaments,[4] keratocytes[3] as well as MDCK cells subjected to traditional scratch wound assays.[37] While it is not entirely clear how local coordination is established in confluent cell populations, we provide experimental and numerical evidence of a quantitative relationship between rotational coordination in confined environments and spatial correlations in the dynamics of unconfined populations. We have established that if the disc radius is smaller or of the order of the unconfined correlation length then a global rotational order is achieved. For larger disks the dynamics is however similar to the unconfined case, exhibiting local streams and curls but no global coordination. These results are in strong agreement with those of similar experiments performed in fibronectin channels;[30] a strong translational order was achieved within channels whose width was smaller than the correlation length but not within wider channels. This similarity is most likely due to the fact that translations and rotations are the two modes of displacements that preserve the relative distances between cells. Both of them therefore enable the population to migrate on the substrate without the requirement of cell–cell junction remodeling.

We postulate that cells on the edge (that experience asymmetric cell adhesion as well as higher confinement) migrate faster and are also guided along the edge of the pattern.[47]

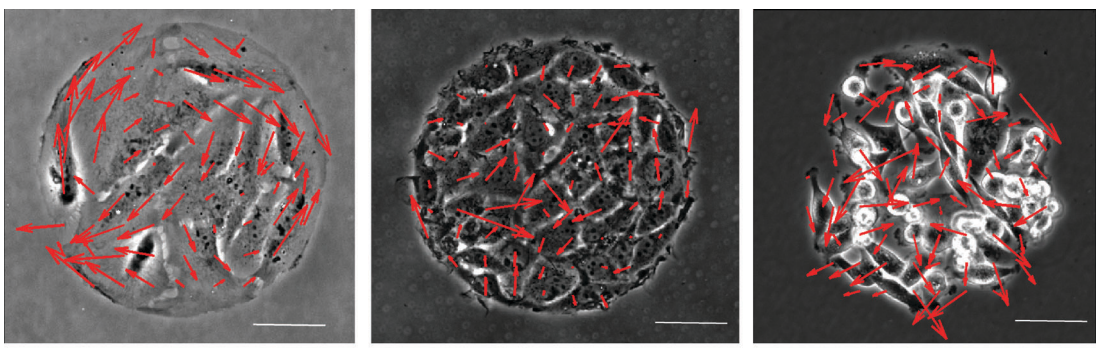

Fig. 6 PIV analysis of the collective behavior of (a) MCF-10A, (b) MCF-7, and (c) MDA-MB-231 on circular fibronectin patterns with a diameter of 200 μm. While MCF-10A shows some order at the pattern edge, MCF-7 and MDA-MB-231 migrate randomly. Scale bar = 50 μm.

Once confluence is reached, the outer cells continue to follow this guidance, while their directional migration is transmitted to the inner cells through cell–cell contacts. The natural correlation length of unconfined monolayers essentially characterizes how far the directional cue from the edge can penetrate into the population. This explains why discs smaller than the correlation length fully coordinate, whereas larger discs cannot. We believe that the strong persistence of the rotational movement is not observed below confluence because of the high frequency of cell divisions and the progressive invasion of available free space. Such dynamics slow down at confluence and a persistent rotational order can be maintained, depending on the population size. The collective rotation behavior observed on circular patterns is also consistent with the 'coherent angular motion' (CAM) observed in epithelial cells cultured in 3D collagen gels, in which the intercellular contacts induce similar polarization of cells[34] within populations of about ~10–15 cell diameters. Even though cell–cell interactions appear to be a key player in the establishment of CAM, the presence of cryptic lamellipodium as previously described[48] could also contribute to the initiation of large scale coordinated mechanisms and their maintenance. Further studies should explore the role of lamellipodium formation in collective cell behaviors.

Epithelial-mesenchymal transition (EMT) induced in MDCK cells by overexpressing the transcription factor Snail-1 decreased the ability of cells to undergo persistent collective rotation. The overexpression of Snail-1 downregulates the expression of E-cadherin. Since intercellular adhesion has been shown to regulate cell polarity and force transmission between cells,[21,49,50] it is likely that weak or immature intercellular adhesions would lead to an inefficient transmission of 'contact guidance' cues from the edge of the ECM pattern to the inner cells diminishing their ability to participate in the collective rotation of the epithelial sheet. Supporting evidence for this observation also comes from the fact that CAM is reduced in the presence of function blocking antibodies directed against E-cadherin.[34] In addition to the formation of acini through CAM, collective rotational persistence of cells has also been observed in other important physiological processes such as embryogenesis. For example, the importance of persistence of rotation has been noted in the migration of the dorsal yolk syncytial layer of teleostean yolk cells.[51] The swirling of cells during late gastrulation is centered around the axial domain of the yolk and needs to persist until the first somite stage for proper development. On a shorter spatial and temporal scale, the 90° rotation of ommatidia pre-clusters in the development of a Drosophila eye is vital for the correct configuration of the hexagonal lattice of the eye.[52]

It is accepted that, in general, while cancer cells have a tremendous ability to proliferate they are unable to organize themselves into higher order tissue structures (*e.g.* acini in breast tissue). Our results suggest that the inability of cancerous cells to undergo synchronized collective rotation could be partially responsible for preventing them from forming higher order tissue structures. While MCF-10A (benign) showed signs of collective migration along the border of the fibronectin circle (contact-guidance), MCF-7 and MDA-MB-231 (malignant) showed a completely random migratory behavior that was unaffected by cell density and ECM confinement. These results raise the possibility that collective behavior could be gradually lost as cells evolve to become more malignant.

In conclusion, we have shown that an interplay between cell density, geometrical constraints and intercellular adhesion regulates the synchronized collective rotation behavior observed in epithelial cells. Furthermore, we have validated the use of μCP patterns as a simpler alternative to study collective behavior and 'coherent angular motion' in epithelial cells. Use of such patterns not only provides significant flexibility in precisely controlling and altering the geometrical constraints imposed but also brings along all the advantages of imaging in 2D. Finally, other factors such as substrate elasticity and/or chemical gradients could also play a significant role in determining collective cell behavior. Future work directed at elucidating the influence of each of these factors as well as the interplay between them would paint a complete picture of how collective cell behavior is regulated.

Experimental section

Cell culture

Wild-type MDCK cells and MDA-MB-231 cells were maintained in DMEM (Hyclone) supplemented with 10% FBS (Hyclone) and 1% penicillin and streptomycin. MDCK cells stably overexpressing the transcription factor Snail-1 (MDCK-S1) were kindly provided by Dr Amparo Cano (IIB, CSIC-UAM, Spain). MCF-7 cells were maintained in RPMI media and MCF-10A cells were maintained in MEBM (Clonetics), both containing 10% FBS (Hyclone) and 1% penicillin and streptomycin.

Microcontact printing

PDMS stamps containing raised circular features of varying diameters were prepared from silanized wafers fabricated using soft lithography techniques.[53] Stamps were incubated with a solution of fibronectin (50 μg ml^{-1}, Sigma) mixed with a small amount of Cy3 conjugated fibronectin for ~1 h, washed and air dried. A thin layer of polydimethyl siloxane (PDMS) was spin coated over a 35 mm plastic Petri dish and cured at 80 °C for 2 h. The Petri dishes were exposed to UV for ~30 minutes to activate the surface. The dried stamps were then gently pressed against the activated PDMS surface to transfer the fibronectin. Pattern transfer was confirmed using fluorescence microscopy. Regions outside the patterns were blocked with 0.2% Pluronic F-127 (Sigma) for 30 minutes and washed with PBS before seeding cells. After allowing cells to attach overnight, they were incubated for 1 hour in 20 μg ml^{-1} of DAPI (Sigma) in culture medium, then washed and imaged on a Biostation™ (Nikon) for ~48 hours. We performed control experiments (without UV exposure) and confirmed that the UV exposure did not have adverse effects on cell behavior.

Image analysis

Particle image velocimetry (PIV) was implemented in MATLAB using MatPIV package.[54] Images were subdivided into 32 × 32 pixel interrogation window patterns greater than or equal to 200 μm in diameter. For the 100 μm diameter patterns, an interrogation

window of 16 × 16 pixels was used to increase the number of velocity vectors computed. Density was computed by manually counting the DAPI labeled nuclei. The time point at which cells filled the whole pattern (without any free space) was considered as the start of the confluent phase and was recorded manually from the videos. The density at which confluence was reached was averaged over several circular patterns and used for separating the subconfluent phase from the confluent phase (red vertical line in Fig. 1d and 5b). The nuclei tracking data were collected using the MTrackJ plugin for ImageJ. The order parameter was computed as the absolute value of the sine of the angle that the velocity vector (obtained by PIV) makes with the radius vector. The value was averaged over all the velocity vectors in an image. An order parameter equal to unity means that all the velocity vectors are tangential to the radius vector. The spatial correlation coefficient was calculated using the formula given below:[30]

$$C(\vec{r}) = \left\langle \frac{\langle u^*(\vec{r}' + \vec{r}, t) \times u^*(\vec{r}', t)\rangle_{\vec{r}'}}{[\langle u^*(\vec{r}' + \vec{r}, t)^2\rangle \langle u^*(\vec{r}', t)^2\rangle]^{1/2}} \right\rangle_t \quad (1)$$

where u^* refers to the deviation of the velocity from the mean velocity, $\vec{r}$ is the vector of the coordinates, and t refers to time. The correlation length is the distance ($||\vec{r}||$) where the spatial velocity correlation function becomes zero.

Numerical modeling of the dynamics of cell monolayers

A model of self-propelled cells is used to study the dynamics of cell monolayers in unconfined and confined situations. The algorithm used in this study is based on a Cellular Potts Model[55] and has been described and characterized previously.[40] Cells mechanically interact through adhesion (encompassed in a membrane tension term) and excluded volume interactions, and generate a propulsive force of constant magnitude on their substrate. The polarity of each cell, controlling the direction of its motile force, evolves as a result of a feedback from the cell displacement, with a certain persistence time. The surface energy of cell–cell interfaces, the amplitude of the motile force and the persistence time of the cell polarity directly control the emergence of collective behavior and the correlation length of the cell velocity field under unconstrained conditions. In this study, we chose the simulation parameters in order to simulate a cell population whose unconfined correlation length matches the unconfined correlation length of MDCK cells (about 10 cell diameters). Using the notations previously described,[40] we used surface energy $J = 5$, motile force $\mu = 0.125$ and persistence time $\tau = 10$.

Cells are constrained to move within circular domains of radii ranging from 3 to 25 cell diameters. The density of the cell population is controlled by adjusting the number of cells placed inside the patterns. To model the behavior of wt-MDCK cells, which form cohesive cell populations, the surface energy of the unbounded cell membrane (at the periphery of the population) is set to 5, *i.e.* identical to the surface energy of cell–cell interfaces. To model Snail-1 MDCK cells, the surface energy of the unbounded cell membrane is set to 2, so that cells are encouraged to form free interfaces rather than bind to each other.

Simulations were run up to 10 000 Monte Carlo steps, in order to reach a steady state. For each run, the correlation function and the resulting correlation length were calculated in the steady state (eqn (1)) in order to allow a direct comparison with experimental data.

Acknowledgements

The authors would like to thank Cyprien Gay, René-Marc Mège and James W. Nelson for helpful discussions, Dr Amparo Cano for providing expressing MDCK cells and Mohammed Ashraf from MBI microfabrication facility for fabrication of the wafers. Financial support from the Agence Nationale de la Recherche (ANR 2010 BLAN 1515 and ANR NMVASC 2010-INTB-1502 awarded to B.L.), the Human Frontier Science Program (grant RGP0040/2012) and the Mechanobiology Institute (Team project funding) is gratefully acknowledged. K.D. was funded by a Fulbright scholarship. N.G. wishes to thank the Mayent-Rothschild Foundation for the Visiting Professor grant at the Institute Curie. The research was conducted in the scope of the International Associated Laboratory Cell Adhesion France Singapore (CAFS).

References

1 P. N. Segrè, E. Herbolzheimer and P. M. Chaikin, *Phys. Rev. Lett.*, 1997, **79**, 2574–2577.
2 M. Nagy, Z. Akos, D. Biro and T. Vicsek, *Nature*, 2010, **464**, U890–U899.
3 B. Szabo, G. J. Szollosi, B. Gonci, Z. Juranyi, D. Selmeczi and T. Vicsek, *Phys. Rev. E: Stat., Nonlinear, Soft Matter Phys.*, 2006, **74**, 061908.
4 V. Schaller, C. Weber, C. Semmrich, E. Frey and A. R. Bausch, *Nature*, 2010, **467**, 73–77.
5 G. Gregoire and H. Chate, *Phys. Rev. Lett.*, 2004, **92**, 025702.
6 P. Friedl, J. Locker, E. Sahai and J. E. Segall, *Nat. Cell Biol.*, 2012, **14**, 777–783.
7 T. E. Angelini, E. Hannezo, X. Trepat, M. Marquez, J. J. Fredberg and D. A. Weitz, *Proc. Natl. Acad. Sci. U. S. A.*, 2011, **108**, 4714–4719.
8 C. J. Weijer, *J. Cell Sci.*, 2009, **122**, 3215–3223.
9 V. Lecaudey and D. Gilmour, *Curr. Opin. Cell Biol.*, 2006, **18**, 102–107.
10 M. Behrndt, G. Salbreux, P. Campinho, R. Hauschild, F. Oswald, J. Roensch, S. W. Grill and C. P. Heisenberg, *Science*, 2012, **338**, 257–260.
11 P. Friedl, P. B. Noble, P. A. Walton, D. W. Laird, P. J. Chauvin, R. J. Tabah, M. Black and K. S. Zanker, *Cancer Res.*, 1995, **55**, 4557–4560.
12 B. Ladoux and A. Nicolas, *Rep. Prog. Phys.*, 2012, **75**, 116601.
13 V. Lecaudey and D. Gilmour, *Curr. Opin. Cell Biol.*, 2006, **18**, 102–107.
14 P. Vitorino and T. Meyer, *Genes Dev.*, 2008, **22**, 3268–3281.
15 K. J. Simpson, L. M. Selfors, J. Bui, A. Reynolds, D. Leake, A. Khvorova and J. S. Brugge, *Nat. Cell Biol.*, 2008, **10**, 1027–1038.
16 Y. Kametani and M. Takeichi, *Nat. Cell Biol.*, 2007, **9**, 92–98.

17 A. A. Khalil and P. Friedl, *Integr. Biol.*, 2010, **2**, 568–574.
18 R. Farooqui and G. Fenteany, *J. Cell Sci.*, 2005, **118**, 51–63.
19 P. Rorth, *Annu. Rev. Cell Dev. Biol.*, 2009, **25**, 407–429.
20 J. Ranft, M. Basan, J. Elgeti, J. F. Joanny, J. Prost and F. Julicher, *Proc. Natl. Acad. Sci. U. S. A.*, 2010, **107**, 20863–20868.
21 X. Trepat, M. R. Wasserman, T. E. Angelini, E. Millet, D. A. Weitz, J. P. Butler and J. J. Fredberg, *Nat. Phys.*, 2009, **5**, 426–430.
22 M. R. Ng, A. Besser, G. Danuser and J. S. Brugge, *J. Cell Biol.*, 2012, **199**, 545–563.
23 N. S. Gov, *HFSP J.*, 2009, **3**, 223–227.
24 D. Choquet, D. P. Felsenfeld and M. P. Sheetz, *Cell*, 1997, **88**, 39–48.
25 C. M. Lo, H. B. Wang, M. Dembo and Y. L. Wang, *Biophys. J.*, 2000, **79**, 144–152.
26 D. Riveline, E. Zamir, N. Q. Balaban, U. S. Schwarz, T. Ishizaki, S. Narumiya, Z. Kam, B. Geiger and A. D. Bershadsky, *J. Cell Biol.*, 2001, **153**, 1175–1185.
27 T. E. Angelini, E. Hannezo, X. Trepat, J. J. Fredberg and D. A. Weitz, *Phys. Rev. Lett.*, 2010, **104**, 168104.
28 M. Poujade, E. Grasland-Mongrain, A. Hertzog, J. Jouanneau, P. Chavrier, B. Ladoux, A. Buguin and P. Silberzan, *Proc. Natl. Acad. Sci. U. S. A.*, 2007, **104**, 15988–15993.
29 C. G. Rolli, H. Nakayama, K. Yamaguchi, J. P. Spatz, R. Kemkemer and J. Nakanishi, *Biomaterials*, 2012, **33**, 2409–2418.
30 S. R. K. Vedula, M. C. Leong, T. L. Lai, P. Hersen, A. J. Kabla, C. T. Lim and B. Ladoux, *Proc. Natl. Acad. Sci. U. S. A.*, 2012, **109**, 12974–12979.
31 X. Serra-Picamal, V. Conte, R. Vincent, E. Anon, D. T. Tambe, E. Bazellieres, J. P. Butler, J. J. Fredberg and X. Trepat, *Nat. Phys.*, 2012, **8**, U628–U666.
32 L. Petitjean, M. Reffay, E. Grasland-Mongrain, M. Poujade, B. Ladoux, A. Buguin and P. Silberzan, *Biophys. J.*, 2010, **98**, 1790–1800.
33 M. Tada and C. P. Heisenberg, *Development*, 2012, **139**, 3897–3904.
34 K. Tanner, H. Mori, R. Mroue, A. Bruni-Cardoso and M. J. Bissell, *Proc. Natl. Acad. Sci. U. S. A.*, 2012, **109**, 1973–1978.
35 L. Q. Wan, K. Ronaldson, M. Park, G. Taylor, Y. Zhang, J. M. Gimble and G. Vunjak-Novakovic, *Proc. Natl. Acad. Sci. U. S. A.*, 2011, **108**, 12295–12300.
36 S. Huang, C. P. Brangwynne, K. K. Parker and D. E. Ingber, *Cell Motil. Cytoskeleton*, 2005, **61**, 201–213.
37 P. Rosen and D. S. Misfeldt, *Proc. Natl. Acad. Sci. U. S. A.*, 1980, **77**, 4760–4763.
38 M. Reffay, L. Petitjean, S. Coscoy, E. Grasland-Mongrain, F. Amblard, A. Buguin and P. Silberzan, *Biophys. J.*, 2011, **100**, 2566–2575.
39 E. Ben-Isaac, Y. Park, G. Popescu, F. L. Brown, N. S. Gov and Y. Shokef, *Phys. Rev. Lett.*, 2011, **106**, 238103.
40 A. J. Kabla, *J. R. Soc., Interface*, 2012, **9**, 3268–3278.
41 J. P. Thiery, *Curr. Opin. Cell Biol.*, 2003, **15**, 740–746.
42 E. Batlle, E. Sancho, C. Franci, D. Dominguez, M. Monfar, J. Baulida and A. Garcia De Herreros, *Nat. Cell Biol.*, 2000, **2**, 84–89.
43 S. Vega, A. V. Morales, O. H. Ocana, F. Valdes, I. Fabregat and M. A. Nieto, *Genes Dev.*, 2004, **18**, 1131–1143.
44 M. Haraguchi, T. Okubo, Y. Miyashita, Y. Miyamoto, M. Hayashi, T. N. Crotti, K. P. McHugh and M. Ozawa, *J. Biol. Chem.*, 2008, **283**, 23514–23523.
45 H. Peinado, E. Ballestar, M. Esteller and A. Cano, *Mol. Cell. Biol.*, 2004, **24**, 306–319.
46 C. G. Rolli, T. Seufferlein, R. Kemkemer and J. P. Spatz, *PLoS One*, 2010, **5**, e8726.
47 R. A. Desai, L. Gao, S. Raghavan, W. F. Liu and C. S. Chen, *J. Cell Sci.*, 2009, **122**, 905–911.
48 R. Farooqui and G. Fenteany, *J. Cell Sci.*, 2005, **118**, 51–63.
49 J. S. Ehrlich, M. D. H. Hansen and W. J. Nelson, *Dev. Cell*, 2002, **3**, 259–270.
50 A. Saez, E. Anon, M. Ghibaudo, O. du Roure, J. M. Di Meglio, P. Hersen, P. Silberzan, A. Buguin and B. Ladoux, *J. Phys.: Condens. Matter*, 2010, **22**, 194119.
51 L. A. D'Amico and M. S. Cooper, *Dev. Dyn.*, 2001, **222**, 611–624.
52 D. Gubb, *Int. J. Dev. Biol.*, 1998, **42**, 369–377.
53 D. Qin, Y. Xia and G. M. Whitesides, *Nat. Protocols*, 2010, **5**, 491–502.
54 J. K. Sveen, http://folk.uio.no/jks/matpiv/Download/, 2006.
55 F. Graner and J. A. Glazier, *Phys. Rev. Lett.*, 1992, **69**, 2013–2016.

